Precession-forced asymmetric continental heating shapes ENSO variability

Yufei Liu[1], Hu Yang[1*], Haowen Dang[2], Gerrit Lohmann[3], Tao Lian[4], Zhengyao Lu[5], Xiaoxu Shi[1], Jiping Liu[1], Hang Wang[1], Feng Jiang[1], Xinyue Deng[1], Xiaoming Hu[1], Dake Chen[1,4,6]

[1]School of Atmospheric Sciences, Sun Yat-sen University, and Southern Marine Science and Engineering Guangdong Laboratory (Zhuhai), China
[2]State Key Laboratory of Marine Geology, Tongji University, Shanghai, China
[3]Alfred Wegener Institute, Helmholtz Centre for Polar and Marine Research, Bremerhaven, Germany
[4]Second Institute of Oceanography, Hangzhou, China
[5]Department of Physical Geography and Ecosystem Science, Lund University, Lund, Sweden
[6]School of Oceanography, Shanghai Jiao Tong University, Shanghai, China

~~Precession affects ENSO variability, which tends to be strong during periods of austral summer perihelion, as in present-day. Asymmetric continental heating between Afro–Eurasia and Australia continents at perihelion and aphelion migrate the warm pool. The zonally migrated warm pool shape the Pacific east-west thermal contrast, altering the threshold for triggering the ENSO events.~~

*Corresponding author

Corresponding author: Hu Yang, yanghu@sml-zhuhai.cn

Abstract

~~Geologic and modelling evidence reveals that the ENSO is strongly affected by the precession of the Earth's rotation axis~~Geological records and climate modeling evidence indicate that the El Niño–Southern Oscillation (ENSO) is strongly modulated by Earth's axial precession, yet the mechanisms remain unclear due to interactions among multiple forcings. Using high-resolution ~~model simulationsreconstructing the ENSO activity~~ climate simulations, we reconstruct ENSO variations across a full precessional cycle~~, we find~~ . Our results reveal that ENSO is ~~strongest during austral summer perihelion, as today. This behavior arises from asymmetric continental heating: austral summer perihelion introduces strong warming on Australia ,~~ more active when perihelion coincides with austral summer and aphelion with boreal summer, consistent with the orbital configuration of the present-day climate. Through diagnostics of background mean climate evolution and ENSO-related feedback processes, we propose that precession-scale modulations in ENSO variability are governed by east–west asymmetric continental warming. When perihelion occurs during austral summer and aphelion during boreal summer, pronounced warming emerges over Australia (east of the Indo-Pacific ~~ITCZ. Because deep convection favors the warmest areas, this causes the ITCZ and the Warm Pool to shift eastwards. As a result, the Pacific's east-west thermal contrast is reduced, lowering the threshold for oscillations of convection and amplifying ENSO activity. In contrast, boreal summer perihelion warms Afro-Eurasia, shifts the ITCZ westward and weakens ENSO~~ Intertropical Convergence Zone (ITCZ)), whereas relative cooling prevails over the Afro–Eurasian continents (west of the Indo-Pacific ITCZ). This east–west thermal contrast drives an eastward shift of the ITCZ and its coupled Walker circulation, accompanied by weakened trade winds, a shallower ocean mixed layer, and enhanced upper-ocean stratification. These changes reduce the thermal inertia of the warm pool, allowing even moderate climate noise to trigger the Bjerknes feedback (including wind and thermocline feedbacks), ultimately magnifying ENSO variability under precessional phases analogous to the modern configuration. Conversely, when perihelion falls in boreal summer and aphelion in austral summer, cooling over Australia and warming over Afro–Eurasian continents force westward displacements of the ITCZ and Walker circulation, strengthen trade winds, force a deeper mixed layer and reduced upper-ocean stratification, suppressing the Bjerknes feedback, thereby dampening ENSO activity during precessional phases corresponding to the Early Holocene. Proxy records ~~across~~ from the Indo-Pacific ~~support this changes in climate state. Understanding asymmetric continental heating helps us link astronomical modulation to ENSO behaviorand improve long-term predictions of tropical climate change~~region support these shifts in climatic regimes. This mechanism of zonal asymmetric continental warming establishes a physical link between astronomical precessional forcing and ENSO behavior, and may provide insights to improve assessments of long-term tropical climate variability.

Plain Language Summary

Observations and climate reconstructions indicate that ENSO is ~~not only affected~~ affected not only by anthropogenic warming but also ~~astronomical cycle~~by astronomical cycles, especially precession. Understanding this long-term behavior is critical for understanding the current state of ENSO and predicting its future. Using ~~~10,~~approximately 10,000 ~~year~~ years of simulations, we ~~have reconstructed~~ reconstruct tropical climate across a full precession cycle ~~tropical climate with~~ at unprecedented resolution. Our results reveal that ~~current~~ present-day ENSO activity is relatively strong ~~in an astronomical~~ within the precession cycle. This ~~is due to~~ arises from asymmetric heating between the ~~Afro-Eurasian~~ Afro–Eurasian and Australian continents at perihelion and aphelion, which ~~shapes the background climate and alters the threshold required to trigger ENSO development. This previously unknown mechanism, validated by geological records across the~~ reorganizes the tropical Pacific mean state and modifies the efficiency of coupled ocean–atmosphere feedbacks that shape ENSO variability. This model-diagnosed pathway, together with geological records that are consistent with the associated Indo-Pacific ~~region, provides the missing~~

~~link between astronomical forcing~~ mean-state and ENSO-variability changes, helps link astronomical forcing to tropical climate variability.

1 Introduction

As the primary driver of global ~~inter-annual~~ interannual variability (Bjerknes, 1969a; Zhang et al., 1997), ~~the El Niño-Southern Oscillation (ENSO)~~ ENSO profoundly influences global climate patterns, ecosystems, and economic activities (Bjerknes, 1966; C. Wang et al., 2017). Modern observations and numerical simulations suggest that anthropogenic warming may amplify ENSO extremes (Timmermann et al., 1999; Cai et al., 2015). However, on longer timescales, other climate forcings also significantly modulate ENSO variability (Liu et al., 2014). For instance, during ~~the~~ geologic warm periods, such as the Holocene and the Last Interglacial, evidence indicates that ENSO activity was weaker than today (Shulmeister & Lees, 1995; Sandweiss et al., 1996; Hewitt & Mitchell, 1998; Rodbell et al., 1999; Sandweiss et al., 2001; McGregor & Gagan, 2004; Conroy et al., 2008; Leduc et al., 2010; Salau et al., 2012; Emile-Geay et al., 2016; Tian et al., 2017). The contrast between stronger ENSO under modern warming and weaker ENSO during past warm periods highlights the complexity of ENSO responses. Understanding the evolution and underlying mechanisms of ENSO is therefore crucial for improving predictive capabilities and informing adaptation strategies under ongoing global change (Cai et al., 2021; Lee et al., 2022).

Proxy records (Tudhope et al., 2001; Koutavas & Joanides, 2012; S. Chen et al., 2016; Barr et al., 2019; Zhou et al., 2022) and model simulations (clement et al., 1999; Bush, 1999; Roberts et al., 2007; An et al., 2018) indicate ~~a~~ weaker ENSO during the ~~Early~~ Early- to mid-Holocene, followed by a gradual intensification lasting several millennia (Moy et al., 2002; Lawman et al., 2022; Lu et al., 2025). Sensitivity experiments isolating orbital variations from other climate forcings identify changes in Earth~~'~~'s orbit, particularly precession (Clement et al., 2000; Moy et al., 2002; Otto-Bliesner et al., 2003; Liu et al., 2003; Timmermann et al., 2007; Chiang et al., 2009; Luan et al., 2012; Braconnot et al., 2012; White et al., 2018; Lu et al., 2019), as the primary driver of this long-term ENSO evolution. Both transient (clement et al., 1999; Clement et al., 2000; Timmermann et al., 2007; Liu et al., 2014; An et al., 2018; Lu et al., 2019; Di Carlo et al., 2021) and time-slice (Otto-Bliesner, 1999; Bush, 1999; Otto-Bliesner et al., 2003; Brown et al., 2006, 2008; Zheng et al., 2008; Chiang et al., 2009; Luan et al., 2012; Salau et al., 2012; Karamperidou et al., 2015; Tian et al., 2017) simulations were performed to understand the dynamics of orbital-scale ENSO ~~activities~~variability. These studies suggest that precession ~~modulate~~ modulates the background climate (clement et al., 1999) ~~, and influence~~ and influences ENSO through complex dynamics, ~~such as~~ including frequency locking (Chang et al., 1994; Liu et al., 2003) and nonlinear resonance (Tziperman et al., 1994; Jin et al., 1994). In particular, weakened ENSO is thought to depend on a La ~~Niña-like background climate~~ Niña-like background climate (Hewitt & Mitchell, 1998; Bush, 1999; Sha et al., 2024), characterized by an enhanced East Asian summer monsoon (Liu et al., 2000, 2003; Pausata et al., 2017; Tian et al., 2017; L. Chen et al., 2019), strengthened Walker circulation (Bush, 1999), and intensified eastern Pacific upwelling (Loubere et al., 2003). ~~Nevertheless, a clear understanding of precession's influence on ENSO remains challenging due to several factors: ENSO '~~More generally, previous studies have shown that external forcing reorganizes the tropical Pacific mean state through changes in Walker circulation strength (P. DiNezio et al., 2011; P. N. DiNezio et al., 2013), warm-pool and ITCZ shifts (Pontes et al., 2022; Thirumalai et al., 2024; Molina et al., 2026), mixed-layer depth (MLD) (Thirumalai et al., 2024), wind-stress anomaly structure (Stuivenvolt-Allen et al., 2025), and upper-ocean stratification (Cai et al., 2018; Tuckman & Yang, 2026). These mean-state changes regulate the efficiency of coupled ocean–atmosphere feedbacks that control ENSO growth, highlighting that ENSO's response to external forcing depends on the tropical Pacific mean state and multiple coupled feedback processes (P. DiNezio et al., 2010; P. N. DiNezio et al., 2012; Fedorov et al., 2020; Cai et al., 2021).

Yet the mechanisms linking orbital forcing, especially precession, to ENSO variability remain poorly constrained. Progress has also been limited by ENSO's high sensitivity to internal variability~~;~~, the relatively weak precession signal ~~in Holocene~~ during the Holocene that is often confounded by other forcings~~;~~, and the coarse resolution of many prior simulations, which may ~~limits~~ limit the ability to capture ~~the~~ complex equatorial current systems and active ~~air-sea interaction~~ air–sea interactions in the deep tropics. ~~Furthermore,~~ Consequently, two key mechanistic questions remain unresolved: How does precession ~~induce a La Niña-like background climate in the early Holocene? And why does such a La Niña-like pattern suppress ENSO activity? To fill these gaps~~reorganize the tropical Pacific mean state? And how do those mean-state changes alter the efficiency of coupled ocean–atmosphere feedbacks and ultimately modulate ENSO amplitude? To address these questions, this study used state-of-the-art climate model simulations to recover ENSO activity over the entire precession cycle using unprecedentedly high-resolution ~~runs of ~10,~~simulations spanning ~10,000 years. This allows us to obtain a full picture of how precession ~~affect~~ affects ENSO behavior. In addition, given that precession is the primary driver of Holocene climate variability (Liu et al., 2014), we also synthesize available ENSO-sensitive proxy records across the Indo-Pacific region to corroborate the trends revealed by the simulations. With these efforts, we find that precession-forced asymmetric continental heating ~~shapes the~~ modulates ENSO variability by ~~altering the threshold of east-west oscillation of deep convection in the Pacific~~reorganizing the tropical Pacific mean state and regulating the efficiency of the coupled Bjerknes feedback loop.

2 Methods

Model Simulations

Previous paleoclimate reconstructions and numerical simulations often considered multiple external forcings, making it difficult to isolate the specific role of individual factors. To specifically assess the impact of precession on ENSO activity, we conducted 24 time-slice simulations reconstructing a full precessional cycle ~~(the precessional phase varies from 0° to 360° in 15° intervals)~~ using the Alfred Wegener Institute Earth System Model (AWI-ESM) (Sidorenko et al., 2015). ~~In particular~~The precessional phase was varied from 0° to 345° in 15° increments. In this framework, a precessional phase of ~~90°~~ 90° corresponds to perihelion at the boreal summer solstice, ~~while phase of 270° represents~~ whereas a phase of 270° corresponds to perihelion at the austral summer solstice. Each simulation was ~~run~~ integrated for 400 years~~, and the final 200 years, after the tropical climate equilibrated, were used to represent the mean climate for each precession phase. This~~. After the tropical climate had equilibrated, the final 100 years were used for the ENSO and mean-state analyses presented in this study. This design allows us to systematically assess ENSO characteristics under varying seasonal distributions of insolation driven by precession (Milankovitch, 1941). The main boundary conditions of the 24 experiments are as follows. Greenhouse-gas concentrations, land-sea distribution, and ice sheet extents were held fixed at pre-industrial conditions. Orbital parameters were prescribed with eccentricity fixed at 0.058 to amplify the precessional insolation contrast, consistent with previous idealized orbital experiments (Yang et al., 2025), and obliquity fixed at 24.50°; only the longitude of perihelion was varied across the 24 time slices. All other boundary conditions follow the AWI-ESM configuration described by Yang (Yang et al., 2024).

~~To diminish the impact of internal climate variability on our results, we adopt a~~ The high eccentricity (0.058) ~~in our simulations, which~~ enhances the detectability of the precession imprint on ~~the~~ tropical Pacific variability and diminishes the impact of internal climate variability on our results. Considering that this design may amplify the precessional forcing, additional experiments with a lower eccentricity (0.02) ~~was~~ were conducted to validate the robustness of our results (see Supplementary Figure S2). Furthermore, to realistically simulate tropical Pacific variability, particularly ENSO dynamics, the model employs a relatively high resolution of up to 25 km near the equator (see Supplementary Figure S1). This resolution effectively improves the representation of ENSO-related ~~ocean-atmosphere~~ ocean–atmosphere coupling (Rackow et al., 2018). ~~Detailed experimental settings are described in Yang et al.~~

Data Analyses

Assessing ENSO ~~Variability and Dynamics~~variability

To evaluate ENSO variability across precessional phases, we ~~analyze~~ first examine the longitude–precession distribution of equatorial Pacific sea surface temperature ~~anomalies (SSTAs) in the Niño 3 region~~ (SST) anomaly (SSTA) standard deviation (Figure 1a). Interannual variance is largest in the eastern equatorial Pacific; therefore, we use the Niño3 region (5°S–5°N, 150°W–90°W) as the primary ENSO index (Trenberth & Stepaniak, 2001). Monthly SST anomalies are calculated relative to each experiment's climatological seasonal cycle over the final 100 years after removing linear trends. The Niño3 index is defined as the three-month running mean of Niño3 SST anomalies. Sensitivity tests using the Niño3.4 and Niño4 regions (not shown) confirm that the main conclusions are insensitive to the choice of ENSO index region. ENSO amplitude is quantified as the standard deviation of the Niño3 index, with 95% confidence intervals estimated from the chi-square distribution (Supplementary Figure S3b). El Niño and La Niña events are identified when the three-month running-mean Niño3 SSTA exceeds +0.5 K or falls below −0.5 K for at least five consecutive overlapping three-month periods (Supplementary Figure S3a,d,e). Power spectral analysis of the Niño3 index is used to characterize ENSO frequency (Supplementary Figure S3c). For the representative weak and strong precessional phases (90° and ~~apply power spectral analysis to characterize the ENSO frequency (Figure 1a). Changes in the position of the~~ 270°), we also perform lead–lag correlation and El Niño composite analyses to examine ENSO life-cycle evolution. These event-scale diagnostics characterize differences in ENSO life-cycle evolution and coupled ocean–atmosphere feedback between the 270° and 90° phases (figures not reproduced here).

Diagnosing precession-driven mean-state changes

To diagnose how precession reorganizes the tropical Pacific mean state, we analyze the zonal migration of the Indo-Pacific ~~ITCZ are tracked by calculating the precipitation-weighted zonal centroid (Figure 1b), defined as the average longitude of grid points where annual mean precipitation exceeds 5 mm/day. To investigate the influence of precessional forcing on energy distribution, we perform an Empirical Orthogonal Function analysis on~~ thermal equator and ITCZ using empirical orthogonal function (EOF) analysis of tropical moist static energy (MSE) ~~variability~~ fields from the 24 precession experiments, treating precession phase as the temporal dimension (Neelin & Held, 1987) (Figure~~4). This approach identifies dominant spatial patterns of MSE variability, linking them to changes in ocean-atmospheric circulation and ENSO dynamics. Detailed calculation methods~~ 3). The zonal migration of the ITCZ serves as the primary indicator of tropical atmospheric reorganization associated with precession. Detailed definitions of MSE and the EOF methodology are provided in the Supplementary Information.

Diagnosing coupled-feedback responses to mean-state changes

To trace the pathway linking tropical Indo-Pacific mean-state reorganization to ENSO variability changes, we diagnose two sets of quantities across the 24 precession experiments (Figure 4a–l). The first set characterizes the mean-state response to precessional forcing, including the Walker-circulation center longitude, equatorial zonal wind stress (τ_x), ITCZ and Indo-Pacific Warm Pool (IPWP) positions, MLD, and upper-ocean stratification (Cai et al., 2018). The second set characterizes how mean-state changes influence ENSO development. These diagnostics include westerly wind burst (WWB) intensity, a regional warm-water volume (WWV) proxy based on equatorial Z_{20} (depth of the 20°C isotherm), and the three components of the Bjerknes feedback together with their product (integrated Bjerknes loop gain, $BJ = \mu\beta\alpha$): atmospheric wind feedback (μ), ocean dynamical response (β), and thermocline feedback (α) (Bjerknes, 1969b; Jin et al., 2006; Lübbecke & McPhaden, 2013; Deppenmeier et al., 2016). Detailed definitions, calculation methods, regional domains, and uncertainty estimates for all diagnostics are provided in the ~~supplementary materials, section on data analysis methods~~Supplementary Information.

Comparison between ~~Simulations~~ simulations and ~~Geological Archives~~geological archives

Despite being idealized, our simulations allow comparison of ENSO variability between precessional phases ~~90° and 270° with Early Holocene-present~~ 90° and 270° with Early Holocene–Late Holocene geological records, as precession ~~is confirmed as the dominant~~ has been identified as an important driver of Holocene ENSO (Lu et al., 2019). Accordingly, we compiled multiple Holocene ENSO ~~proxies - including~~ proxies—including sediment reflectance, varve thickness, grain size, sterol biomarkers, and foraminiferal $\delta^{18}O$ ~~variance - which~~ variance—which capture ENSO variability changes (Supplementary Figure S9). Paleoclimate records also provide a practical way to reconstruct background climate, with Holocene variability also largely governed by precession (Liu et al., 2014). By comparing reconstructed precipitation anomalies and SSTAs between ~~early and late~~ the Early and Late Holocene with simulated anomalies under precessional extremes (~~90°–270°~~90°–270°), we assess the consistency of modeled ~~climate state trend~~ climate-state trends with geological evidence (~~Figures 5).~~ Figure 5). In Figure 5, 27°C SST isotherms outline IPWP boundaries at the 90° and 270° extremes for comparison with proxy reconstructions. Detailed methods are provided in the Supplementary ~~Materials~~Information.

3 Results

Precession ~~modulate~~ modulates ENSO activity

Unlike previous simulations that include multiple external forcings, our results from simulations focused solely on precession indicate that the strength of ENSO activity, estimated as the standard deviation of equatorial ~~sea surface temperature anomalies (SSTAs)~~SSTAs, varies throughout a precessional cycle. We find that ENSO variability is most pronounced in the ~~Niño3~~ Niño3 region (Figure 1a), ~~peaking~~ where simulated interannual SST variance is largest in the eastern equatorial Pacific. Therefore, we use Niño3 as our primary index to quantify the ENSO activities. ENSO amplitude peaks at a precessional phase of approximately 270°~~–~~–285°, with perihelion/aphelion ~~occurs~~ occurring in austral summer/winter. In contrast, the weakest ENSO variability occurs at a precessional phase of approximately 90°~~–~~–105°, with perihelion/aphelion ~~occurs~~ occurring in boreal summer/winter. ~~This pattern~~ The simulated ENSO amplitude increases by $106 \pm 4\%$ at 270° compared to 90°.

This phase dependence is consistent with earlier ~~modelling~~ modeling studies, indicating relatively weak ENSO during the early Holocene (Lu et al., 2018) and the Last Interglacial (Salau et al., 2012), when the precession phases were around 90°~~-~~–120° (Bush, 1999; Liu et al., 2000; Otto-Bliesner et al., 2003; Salau et al., 2012). ~~The simulated ENSO amplitude increases by $106 \pm 4\%$ at 270° compared to 90°.~~ Previous studies reported relatively smaller ENSO variations during the Holocene based on paleoclimate records (15%~~-60~~–60%) (Tudhope et al., 2001; Moy et al., 2002; McGregor & Gagan, 2004; Conroy et al., 2008; Emile-Geay et al., 2016; White et al., 2018) and numerical simulations (2%~~-30%)~~ –30%) (Liu et al., 2003; Salau et al., 2012; Liu et al., 2014; Karamperidou et al., 2015; Tian et al., 2017). These discrepancies in ENSO amplitude may be attributed to the higher eccentricity in our experiments (0.058), which exceeds the Holocene eccentricity value (approximately 0.02). Additional simulations with low eccentricity (0.02) yield a $59 \pm 4\%$ increase in ENSO amplitude (Supplementary Figure S2), showing the same trend

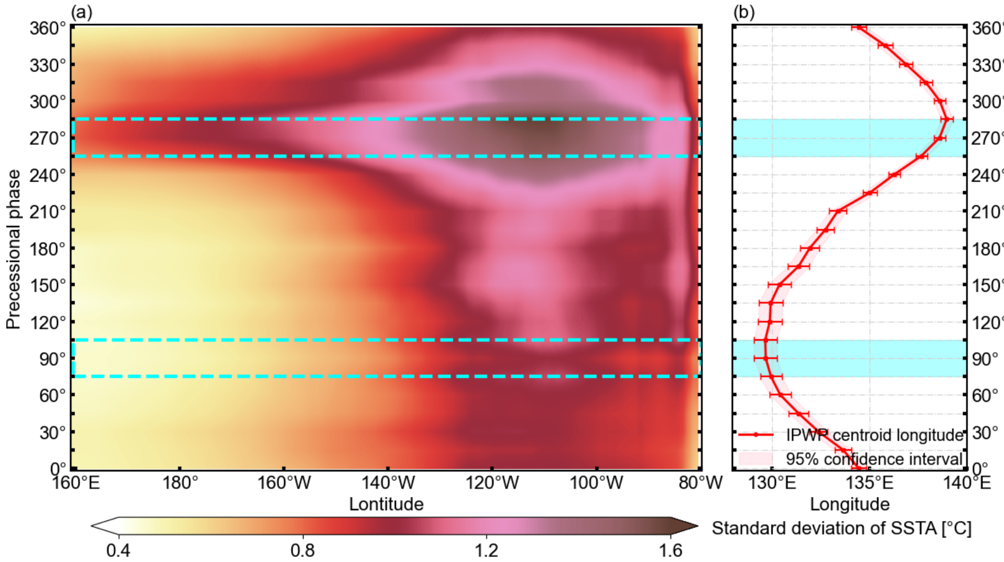

Figure 1. Simulated El Niño–Southern Oscillation strength and zonal position of the Indo-Pacific Warm Pool over a precessional cycle (eccentricity = 0.058). (a) Standard deviation of equatorial (5°S–5°N) tropical Pacific sea surface temperature anomalies. The x-axis is longitude, the y-axis is precession phase, and shading shows El Niño–Southern Oscillation strength. Blue dashed lines mark extreme El Niño–Southern Oscillation phases: ∼270° (strongest El Niño–Southern Oscillation when perihelion/aphelion occur in austral summer/winter) and ∼90° (weakest El Niño–Southern Oscillation when perihelion/aphelion occur in boreal summer/winter). (b) Zonal migration of the Indo-Pacific Intertropical Convergence Zone or Indo-Pacific Warm Pool, defined as the precipitation-weighted longitude where annual mean precipitation exceeds 5 mm day^{-1} (green contour in Supplementary Figure S4; see Section 2). Blue shading highlights the precession phases corresponding to the easternmost (270°) and westernmost (90°) Intertropical Convergence Zone positions.

but with smaller magnitude than the 0.058-eccentricity runs. ~~Power spectral analysis further indicates that precession affects~~

In addition, precession influences not only ENSO amplitude but also ~~its frequency: the simulated ENSO frequency is 68 ± 3% higher~~ ENSO frequency and event occurrence (Supplementary Figure S3). Across the 24 experiments, both El Niño and La Niña events are more frequent near 255°–300° and less frequent near 75°–135° (Supplementary Figure S3a). In the representative weak and strong phases, the 90° experiment yields 19 El Niño and 19 La Niña events, whereas the 270° experiment yields 31 and 25 events, respectively. Power spectra likewise indicate a shift toward shorter ENSO timescales near 255°–300°, with the dominant spectral peak shifting from about a 6-year period at 90° to about 4 years at 270° (Supplementary Figure S3c). The corresponding Niño3 time series illustrate this contrast, with more frequent and larger-amplitude events under 270° than under 90° (~~as shown in Supplementary FigureS3). The coherent modulation of~~ Supplementary Figure S3d,e). Together, these results demonstrate that precession coherently modulates both ENSO amplitude and frequency ~~across the precession cycle~~ (Lu et al., 2025)~~provides strong evidence that precession alter ENSO activities~~. To understand this response, we next examine how precession reorganizes the tropical Pacific mean state.

Coupling of the tropical ~~mean-state~~ mean state and ENSO activity

To investigate how ENSO responds to precession, we first examine the variations in atmospheric and oceanic circulation throughout the precessional cycle. As illustrated in

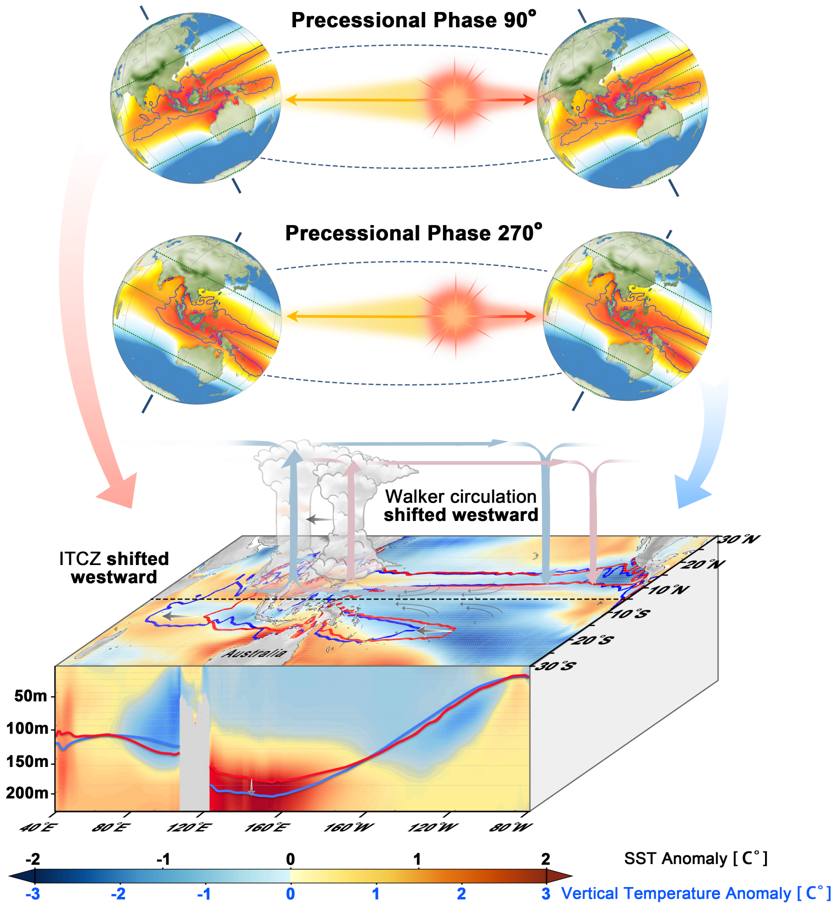

Figure 2. Schematic of background ocean–atmosphere circulation under two precessional phases with extreme El Niño–Southern Oscillation intensity (90° versus 270°). Upper panels show Earth–Sun positions at precessional phases of 90° and 270°. Lower panels show corresponding climate states (90° blue, 270° red): shading indicates horizontal (30°S–30°N) and equatorial vertical (5°S–5°N) ocean temperature anomalies. Due to different thermal inertia between land and ocean, perihelion/aphelion introduce relatively stronger warming/cooling over land than over ocean. This generates an east–west shift of the Indo-Pacific Intertropical Convergence Zone due to the zonally asymmetric land–sea distribution. At a precessional phase of 90°, boreal summer/winter perihelion/aphelion drives relatively stronger warming/cooling over the Afro–Eurasian/Australian continents. The combined zonally asymmetric thermal forcing drives westward shifts (grey arrows) of the Intertropical Convergence Zone (horizontal contours) and Walker circulation (vertical arrows), stronger equatorial Pacific trade winds, and a deeper western Pacific thermocline, favoring weaker El Niño–Southern Oscillation variability. At 270°, austral summer/winter perihelion/aphelion induces opposite shifts, favoring stronger El Niño–Southern Oscillation variability.

Figure 1b, the Indo-Pacific ~~Intertropical Convergence Zone (ITCZ)~~ ITCZ migrates zonally during the precessional cycle, with its westernmost position occurring around 90° (Figure 2). ~~This corresponds to~~ This westward migration of the ITCZ is accompanied by a westward shift ~~in the Walker Circulation~~ of the Walker circulation (Salau et al., 2012; Pausata et al., 2017; Sha et al., 2024). The westward migration of atmospheric circulation ~~leads to a strengthening of~~ strengthens equatorial trade winds in the western Pacific (Zheng et al., 2008; Chiang et al., 2009), while ~~the~~ weakening equatorial westerlies in the Indian Ocean~~weaken~~. These changes in surface winds ~~also cause the position of surface water convergence in the Indo-Pacific Warm Pool (IPWP) to shift westward~~ are also associated with a westward displacement of the IPWP (Linsley et al., 2010), ~~along~~ together with a deepening of the western Pacific thermocline and weaker upper-ocean stratification (Loubere et al., 2003; Pausata et al., 2017; Cai et al., 2018). Geological records indicate higher ocean heat content at precessional phase 90°, supporting a deeper and warmer subsurface thermocline in the IPWP (Jian et al., 2022). In the eastern Pacific, the westward-shifted IPWP and intensified trade winds enhance upwelling in the cold tongue region (see Supplementary ~~Figure S5-S7~~ Figures S5–S7 for atmospheric and oceanic circulation contrasts between the 90° and 270° precessional phases) ~~, generate a La Niña-like~~ (Liu et al., 2014; White et al., 2018; Lu et al., 2019), generating a La Niña-like mean state (Koutavas et al., 2002; Kienast et al., 2006). This mean-state ~~. This~~ configuration corresponds with weakened ENSO activity, as shown in our simulations (Figure 1a). In contrast, when perihelion/aphelion occurs during the austral summer/winter (precessional phase 270°), the IPWP, ITCZ, and Walker ~~Circulation~~ circulation shift eastward (Figure 2). This weakens the equatorial Pacific trade winds, ~~creating~~ enhances upper-ocean stratification, and shallows the mixed layer (Cai et al., 2018, 2021), creating a mean climate state that ~~resemble El Niño~~ resembles El Niño (Sha et al., 2024)~~,~~. This background state is associated with more intense and frequent ENSO events at precessional phase 270° (Figure 1a). Therefore, consistent with previous studies, our simulations suggest that external forcing first reorganizes the tropical Pacific mean state, which provides the background conditions that regulate ENSO variability through changes in coupled ocean–atmosphere interactions (P. N. DiNezio et al., 2012; Fedorov et al., 2020; Thirumalai et al., 2024; Tuckman & Yang, 2026).

~~Changes in mean-state alter the threshold for triggering ENSO events~~

~~ENSO initiation and growth are closely tied to positive ocean-atmosphere feedback associated with tropical Pacific deep convection . During El Niño events, anomalously eastward-extending Indo-Pacific deep convection weakens the Pacific trade winds, allowing Warm Pool waters to move eastward. This, in turn, further reinforces the eastward expansion of deep convection, forming a positive feedback loop . In contrast, during La Niña events, tropical deep convection shifts westward .~~

~~Since deep convection tends to occur where tropospheric moist static energy (MSE) is locally maximized, changes in the zonal MSE distribution under two precessional extreme stateof ENSO intensity (i.e., precessional 90° versus 270°) are examined to understand the different ENSO behavior. In 90°, a stronger east-west MSE difference, associated with a La Niña-like background climate with westward located ITCZ, makes the eastward expansion of deep convection more difficult, reducing the likelihood of triggering the positive feedback (Figure ??a). Conversely, in 270°, a smaller east-west MSE difference, linked to El Nino-like background climate with eastward located ITCZ, allows even small climate noise to more easily initiate the positive feedback loop (Figure ??b). As a result, the east-west MSE difference serves as a reliable diagnostic metric for the frequency and amplitude of ENSO events, as evidenced by its high correlation with the Niño3 index (Figure ??c, d).~~

Asymmetric continental heating as a principal force

Above, we ~~identified that changes in the ENSO-associated mean climate state , such as~~ showed that precession forcing reorganizes the tropical Indo-Pacific mean state, including variations in the ITCZ, surface winds, the Walker Circulation, and the thermocline structure—can influence ENSO activity. Among these internally coupled climate elements, the zonal position of the ITCZ emerges as a key control on the threshold for triggering ENSO events. However, understanding the mechanisms behind these mean-state changes remains challenging due to the inherently coupled nature of tropical ocean-atmosphere dynamics. To clarify the mechanisms that drive changes in the background climate, we investigate potential external causes of the zonal migration of the Indo-Pacific ITCZWalker circulation, MLD, and upper-ocean stratification. To clarify how precession drives these changes, we use the zonal migration of the Indo-Pacific ITCZ as a dynamical indicator, because its position reflects the reorganization of tropical atmospheric circulation and associated oceanic background conditions. The Indo-Pacific ITCZ , a narrow equatorial band of deep convection near the thermal equator, can be objectively identified as the region of maximum MSE over the tropical ocean (Neelin & Held, 1987). To capture characterize its migration pattern, we performed Empirical Orthogonal Function (EOF) an EOF analysis on tropical MSE fields from the 24 precessional experiments, separately for boreal summers and winters.

Precession drives summer and winter. Precession drives the seasonal distribution of insolation by altering the timing of different Earth-Sun Earth–Sun distances (Milankovitch, 1941; Yang et al., 2025). Then, the key question here The key question is how the zonally symmetric insolation variations caused by precession affect the zonal migration of the ITCZ. To understand thisproblemaddress this, we first need to understand recall some basic facts. The apparent movement of the Sun 's position between the Tropic of Cancer and the Tropic of Capricorn generates the annual cycle. From this point of view, seasons are a function of latitude, namely the latitude of the overhead Sun. Precession determines the seasonal timing of the perihelion and aphelion , therefore , it and therefore alters the latitude where at which perihelion and aphelion concentrate insolation (Yang et al., 2025). As shown in Figure 3a,b, at precessional phase 90°, when perihelion occurs during boreal summer, the northernmost latitude receives the maximum solar radiation (magenta dashed line). This generates the strongest continental heating over the Afro-Eurasian Afro–Eurasian landmass to the west of the Indo-Pacific ITCZ. The intensified thermal contrast between the Afro-Eurasian Afro–Eurasian continent and the adjacent ocean basins induces low-level convergence of warm surface air and water moisture toward the landmass, resulting in a westward displacement of the Indo-Pacific thermal equator and ITCZ during boreal summer. Corresponding to boreal summer perihelion, aphelion occurs in austral summer, when the weakest insolation is concentrate concentrated at the southernmost latitude (Figure 3c,d). This forces relatively stronger cooling over the Australian continent at to the east of the Indo-Pacific ITCZ. Similarly, it drives a westward shift of the Indo-Pacific thermal equator and ITCZ during austral summer (the corresponding ITCZ movements are shown in Supplementary Figure S8). Thus, from an annual-mean perspective, the Indo-Pacific ITCZ is positioned farther west during precessional phase 90° compared to than during phase 270° (Figure 3e,f). The westward shift of the Indo-Pacific ITCZ establishes a La Niña-like Niña-like background state under 90°. These changes raise the threshold for ENSO initiation thereby suppress ENSO , associated with weaker ocean–atmosphere coupling and reduced ENSO variability. Conversely, at precessional phase 270°, boreal summer aphelion (Figure 3c,d) enhances relative cooling over the Afro-Eurasian Afro–Eurasian continent to the west of the Indo-Pacific ITCZ, while austral summer perihelion (Figure 3a,b) increases heating over the Australian landmass. This reversed (PC1) continental thermal contrast causes leads to an eastward shift of the ITCZ and IPWP. The resulting El Niño-like background climate promotes stronger atmosphere-ocean Niño-like background climate likely favors stronger atmosphere–ocean coupling in the tropical Pacific , lowers the threshold for triggering ENSO events, and enhances and enhanced ENSO activity.

Hence, we propose that the perihelion and aphelion combined asymmetric continental heating —especially over Afro-Eurasia and Australia— over Afro–Eurasia and Australia acts as a key external driver inducing zonal shifts of the Indo-Pacific ITCZ. These zonal shifts reorganize the tropical background state, including ocean-atmosphere feedback related to

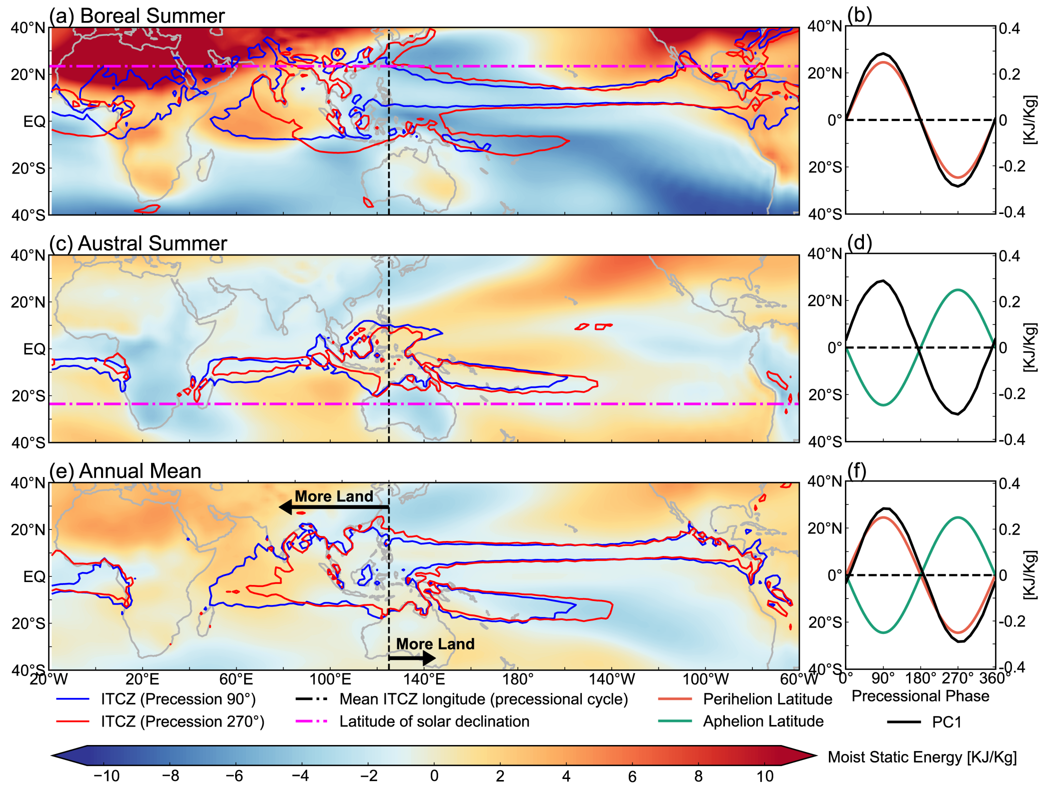

Figure 3. Empirical orthogonal function analysis of boreal summer (June–July–August; a, b), boreal winter (December–January–February; c, d), and annual mean (e, f) moist static energy variability over a precessional cycle (eccentricity = 0.058). (a, c, e) Color shading shows the spatial patterns of the leading empirical orthogonal function modes, accounting for 96.2%, 61.4%, and 90.8% of the total variance, respectively. Blue and red contours indicate the Indo-Pacific Intertropical Convergence Zone positions at precessional phases 90° and 270°, respectively. Magenta dashed lines mark the latitude of overhead Sun. The dashed black line shows the average zonal position of the Indo-Pacific Intertropical Convergence Zone over the precessional cycle. (b, d, f) Time series of the leading empirical orthogonal function mode (black), with orange and green lines marking the latitude of overhead Sun at the time of perihelion and aphelion, respectively (Yang et al., 2024).

~~ENSO, alter the threshold for ENSO initiation, and modulate ENSO variability.~~driver of the changes in background coupling of the tropical mean state, for example, the east–west migration of ITCZ, Walker circulation and the IPWP. Next, we investigate how this mean-state reorganization modifies ocean–atmosphere coupling and ENSO variability.

Tropical Pacific mean-state control of ENSO feedback efficiency

Above, we have demonstrated that precession-induced asymmetric continental heating can reorganize the tropical Pacific mean state, including zonal shifts in the Walker circulation, the ITCZ, the IPWP, and changes in the equatorial thermocline structure. Building on these mean-state changes, we next investigate how the reorganized tropical Pacific background state regulates ENSO variability through changes in air–sea coupling efficiency. Previous studies have shown that ENSO variability depends not only on the magnitude of initial ocean–atmosphere disturbances, but also on the background climate state that determines the efficiency of coupled ocean–atmosphere feedbacks (Molina et al., 2026; Fedorov & Philander, 2001; Cai et al., 2018). The growth of ENSO events is primarily governed by the Bjerknes positive feedback (Jin et al., 2006; Bjerknes, 1969b), which consists of three interconnected processes: the atmospheric response of wind stress to SST anomalies (μ), the dynamical response of the thermocline to wind stress anomalies (β), and the thermodynamic conversion of subsurface ocean temperature anomalies associated with thermocline variations into SST anomalies (α). Together, these feedback components form a positive feedback loop that amplifies initial disturbances and promotes the growth of El Niño and La Niña events.

The efficiency of these coupled feedbacks is highly dependent on the location of the sensitive air–sea coupling region (C. Wang & Picaut, 2004). The most effective coupling generally occurs near the eastern edge of the IPWP rather than within its warmest core (Guilyardi et al., 2009). The warm-pool interior maintains persistent deep convection, where atmospheric convection is frequently active and becomes less sensitive to small SST perturbations because it is constrained by atmospheric stability and moisture availability rather than SST forcing alone. In contrast, the eastern edge of the warm pool is located within an SST range favorable for deep convection (approximately 28°C), where relatively small SST anomalies can induce substantial changes in convection, precipitation, and latent heat release. These atmospheric responses can further modify the Walker circulation and surface wind field, which in turn regulate upper-ocean stratification and MLD and ultimately influence ENSO feedback efficiency (P. N. DiNezio et al., 2012; Fedorov et al., 2020; Cai et al., 2021). Therefore, shifts in the zonal position of the eastern edge of the IPWP relocate the region of maximum air–sea coupling sensitivity. Such changes provide a physical pathway through which external forcing can regulate ENSO variability by modifying coupled feedback efficiency.

The 24 precession simulations reveal a clear orbital modulation of ENSO amplitude (Figure 4). During the strong ENSO phase associated with 255°–300° precession, the Walker circulation and the IPWP shift significantly eastward, accompanied by weakened equatorial easterly wind stress. These atmospheric adjustments are associated with substantial changes in upper-ocean structure, including a shallower mixed layer in the warm pool, enhanced upper-ocean stratification, and a reduced background warm-water reservoir in the western–central Pacific. These changes indicate reduced oceanic thermal inertia, which leads to enhanced sensitivity of SST anomalies to atmospheric perturbations. Meanwhile, WWBs become stronger under this background state. The eastward displacement of the IPWP eastern edge shifts the sensitive air–sea coupling region toward the central Pacific, while the reduced oceanic thermal inertia allows the upper ocean to respond more efficiently to wind perturbations.

Consistent with these mean-state changes, all three components of the Bjerknes feedback increase (Figure 4i–l), with the thermodynamic feedback exhibiting a particularly pronounced enhancement. The atmospheric feedback (μ) increases because SST anomalies more effectively modify atmospheric circulation and wind stress near the displaced warm-pool edge. The dynamical feedback (β) is enhanced because wind stress anomalies more efficiently perturb thermocline depth. In addition, the shallower thermocline and stronger upper-ocean stratification increase the efficiency of converting subsurface ocean temperature anomalies associated with thermocline variations into surface warming or cooling, leading to an enhanced thermodynamic feedback (α). Therefore, the combined Bjerknes feedback gain ($\mathrm{BJ} = \mu\beta\alpha$) reaches its maximum near 270° precession. The strengthened positive feedback loop amplifies initial ocean–atmosphere disturbances and produces larger ENSO variability.

In contrast, ENSO variability is substantially reduced during the precessional phase between 75°–135°. The standard deviation of Niño3 SST anomalies reaches its minimum, while the Walker circulation and IPWP remain shifted westward. Stronger background easterly winds maintain a more stable cold-tongue structure and inhibit the growth of SST anomalies, while the warm pool upper ocean exhibits a deeper mixed layer, weaker stratification, and a larger thermal reservoir. Under these conditions, the efficiency of air–sea coupling decreases. The westward displacement of the IPWP eastern edge reduces

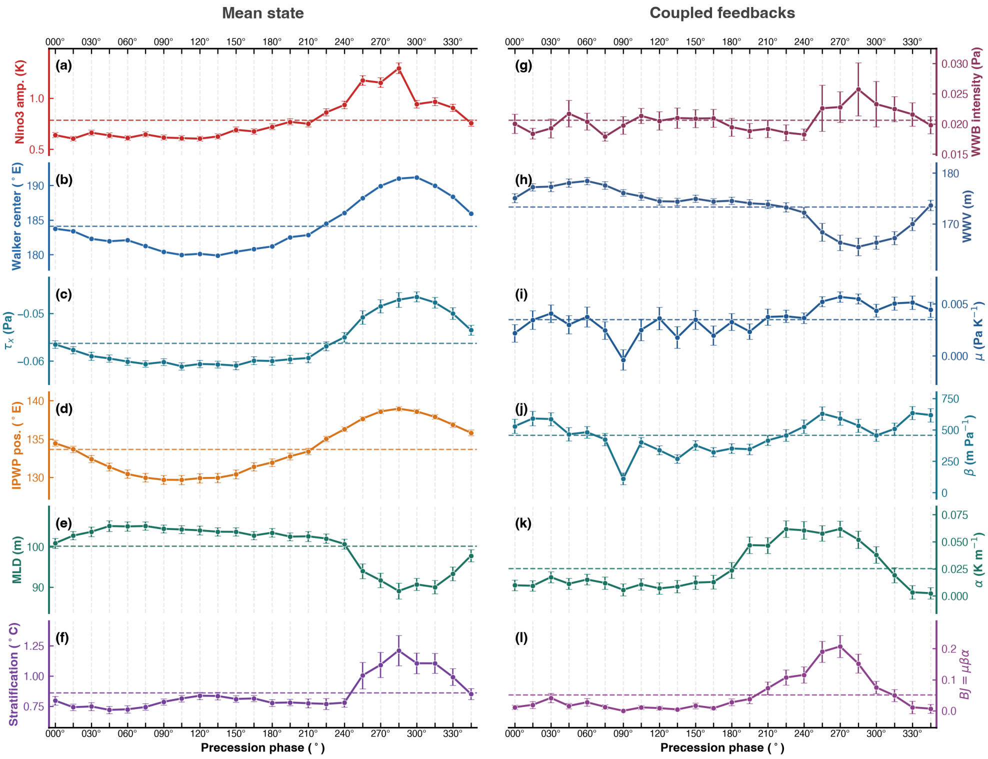

Figure 4. Mean-state and coupled-feedback diagnostics across the 24 precession experiments. Left column (mean state): (a) Niño3 amplitude; (b) Walker-circulation center longitude; (c) equatorial zonal wind stress; (d) precipitation-weighted tropical convection centroid (shared Intertropical Convergence Zone/Indo-Pacific Warm Pool migration surrogate); (e) mixed-layer depth; and (f) upper-ocean stratification. Right column (coupled feedbacks): (g) westerly wind burst intensity; (h) regional warm-water volume proxy based on equatorial Z_{20}; (i) wind feedback μ; (j) ocean dynamical response β; (k) thermocline feedback α; and (l) integrated Bjerknes loop gain $\mu\beta\alpha$. Pearson correlations (r) with Niño3 amplitude are shown in each panel. Strong El Niño–Southern Oscillation phases consistently coincide with an eastward-displaced Walker circulation and warm pool, weaker trade winds, a shallower mixed layer, enhanced upper-ocean stratification, and stronger Bjerknes-loop efficiency. Error bars show 95% confidence intervals where available. Dashed lines denote multi-experiment means. Definitions and calculation methods are summarized in Supplementary Table S3.

the sensitivity of atmospheric convection and wind stress to SST anomalies, weakening the atmospheric feedback (μ). The reduced response of the thermocline to wind forcing decreases the dynamical feedback (β), while the deeper thermocline and weaker stratification inhibit the transfer of subsurface ocean anomalies to the surface, reducing the thermodynamic feedback (α). Consequently, the combined Bjerknes feedback gain (BJ $= \mu\beta\alpha$) reaches a minimum, preventing initial disturbances from undergoing sustained amplification and resulting in weaker ENSO variability.

Together, these results demonstrate that precessional forcing does not regulate ENSO variability simply by shifting the tropical Pacific toward a mean El Niño-like or La Niña-like state. Instead, external forcing (like precession) modifies the background climate state, including the Walker circulation (P. N. DiNezio et al., 2013; Fedorov et al., 2020), IPWP position (Thirumalai et al., 2024; Molina et al., 2026; Pontes et al., 2022), surface wind field, mixed-layer structure, and upper-ocean stratification (Cai et al., 2018; Tuckman & Yang, 2026), thereby regulating the efficiency of tropical Pacific air–sea coupling. These mean-state adjustments collectively modulate the three components of the Bjerknes feedback (μ, β, and α). In our simulations, enhanced upper-ocean stratification plays a particularly important role by strengthening the thermodynamic feedback (α), while the concurrent increase in atmospheric wind feedback (μ) further amplifies the total Bjerknes feedback efficiency. Together, these processes explain the enhanced ENSO variability near the 270° precession phase by establishing a background state with more efficient ocean–atmosphere coupling.

Evidence from geological proxy reconstructions

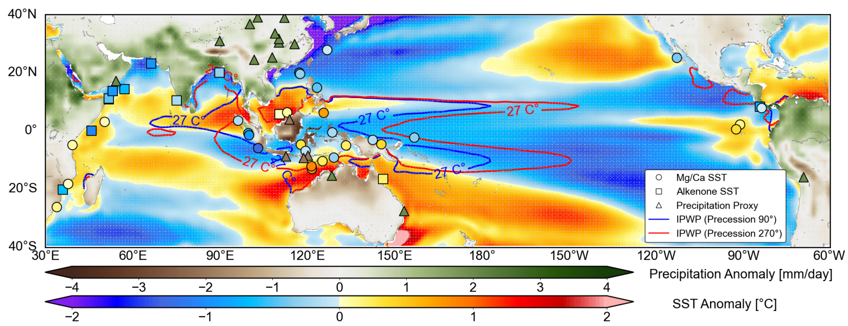

Figure 5. Zonal migration of the Indo-Pacific Intertropical Convergence Zone and Indo-Pacific Warm Pool inferred from climate model simulations and geological records. Shading depicts sea surface temperature anomaly and convective precipitation anomalies between two precessional extreme states of El Niño–Southern Oscillation intensity (precession phases at 90° and 270°). Contours delineate the Indo-Pacific Warm Pool boundaries, defined by the 27°C isotherm, for precession phase 270° (red) and 90° (blue). Symbols on ocean and land denote proxy-reconstructed changes from early to late Holocene: circles indicate sea surface temperature anomalies from Mg/Ca records, squares denote sea surface temperature anomalies from alkenone ($U_{37}^{K'}$) records. Green triangles denote precipitation reconstructions from multiple methods indicating wetter early Holocene conditions relative to the late Holocene, whereas brown triangles imply drier early Holocene conditions. Due to the limited availability of quantitative precipitation reconstructions, these trends are directly taken from previous studies. Matching colors between symbols and background shading reflect consistent trends between proxy reconstructions and model simulations. More detailed information on the sea surface temperature and precipitation proxies can be found in Supplementary Tables S1–S2, respectively.

Having diagnosed the model-based pathway linking precession-driven mean-state reorganization to ENSO variability, we next evaluate whether the simulated ENSO-variability and Indo-Pacific mean-state changes are consistent with geological evidence. Although our precessional experiments represent an idealized framework that simplifies real-world complexity, they still provide valuable insights into ENSO-related climate variability during periods ~~primarily driven~~ strongly influenced by precession. These insights can be evaluated using geological archives, which provide empirical benchmarks for assessing model performance. Notably, ~~the Holocene climate changes is forced primarily~~ Holocene climate change was strongly influenced by a shift in precession phase from 90° to 270°, accompanied by a wealth of proxy-based climate reconstructions (Lu et al., 2018). Multiple proxy-based ENSO variability records consistently indicate weaker ENSO activity during the early to mid-Holocene, followed by a gradual intensification during the late Holocene (Supplementary Figure S9)

(Moy et al., 2002; Conroy et al., 2008, 2009; Koutavas & Joanides, 2012; Emile-Geay et al., 2016; Thompson et al., 2017). Taken together, these observational findings are in good agreement with the simulated response to precession-driven changes in climate.

Paleoclimate records also help assess changes in the mean climate state simulated in our experiments, such as the zonal migration of the ITCZ and the IPWP. ~~Even though~~ Although our experiments amplify the precessional forcing, the sign of the climate ~~changes due to precession should be~~ responses associated with precession is independent of the ~~chosen~~ prescribed eccentricity (Supplementary Figure S2). During the early Holocene, precipitation reconstructions from Southeast Asia and North Africa indicate wetter conditions than in the Late Holocene~~. In contrast, Indonesia and northern Australia were drier~~ , whereas records from Indonesia suggest relatively drier conditions during this period (Figure ~~4~~5). These hydroclimate patterns ~~support our simulated eastward migration of the ITCZ from~~ are broadly consistent with our simulated westward-displaced ITCZ during precession phase 90° (Early Holocene) ~~to~~ and its subsequent eastward migration toward 270° (Late Holocene). In addition to precipitation records, tropical marine sediment cores provide further evidence for changes in Indo-Pacific temperature associated with ITCZ migration. We compiled available SST records derived from Mg/Ca and alkenone across the Indo-Pacific. These data suggest a westward shift of the IPWP during the Early Holocene, as reflected by warmer SSTs in the western IPWP and cooler SSTs in the east, relative to the Late Holocene (Figure ~~4~~5; see also Supplementary Figure S10 for robustness). These multiproxy comparisons provide ~~strong~~ broad empirical support for the simulated shifts in the IPWP and ITCZ from precession ~~90° to 270°~~90° to 270°. We also note that there are some ~~mismatches between simulation and proxies~~regional mismatches between simulations and proxy reconstructions. For example, ~~the reconstructed increased rainfall over northern Australia~~ reconstructed rainfall records from northern Australia indicate wetter conditions during the early Holocene~~is not captured by our simulations , which likely reflects a stronger influence of ENSO events rather than~~ , whereas our simulations show a drying tendency associated with the mean ITCZ position. We attribute this discrepancy to the possibility that northern Australian hydroclimate records capture episodic ENSO-related rainfall variability, rather than solely the mean-state influence of ITCZ migration. The westward-shifted ITCZ and La ~~Niña-like background~~ Niña-like background state during the early Holocene could ~~increase the flood~~ have enhanced the occurrence of extreme rainfall and flooding events in Australia (Denniston et al., 2013; Barr et al., 2019).

Together, these geological constraints provide independent observational support for the simulated precession-driven reorganization of the tropical Pacific mean state, particularly the zonal migration of the ITCZ and the IPWP.

4 Conclusion and Discussion

~~ENSO's nonlinear response to precession forcingis primarily mediated by ocean–atmosphere interactions. Early Holocene ENSO suppression is commonly attributed to a strong~~ Across a full precession cycle, our simulations provide a mechanistic framework for understanding how ENSO variability responds to precessional forcing. We demonstrate that ENSO variability exhibits a pronounced precessional modulation, with the strongest variability occurring around the 270° precession phase (like the modern orbital configuration) and substantially weakened ENSO activity near the 90° phase (like the early Holocene configuration). This modulation arises because precession alters the seasonal and hemispheric distribution of insolation, thereby generating east–west asymmetric continental heating between the Australian and Afro–Eurasian continents and subsequently reorganizing the tropical Indo-Pacific mean state. Specifically, during the 270° precession phase, perihelion occurs in austral summer, resulting in enhanced radiative heating over Australia, which is located to the west of the IPWP. In contrast, during boreal summer, aphelion reduces seasonal radiative heating over the Afro–Eurasian continent, which lies adjacent to the eastern side of the IPWP. This hemispherically asymmetric continental thermal forcing drives a northeastward shift of the

IPWP and the center of deep tropical convection, triggering mean-state adjustments in the ENSO-sensitive western–central Pacific region. These adjustments feature an eastward displacement of the Walker circulation, weakened equatorial trade winds, a shallower mixed layer, reduced upper-ocean WWV, and intensified ocean stratification. Meanwhile, weakened background trade winds favor stronger WWB activity, further modifying the ocean–atmosphere coupling processes that regulate ENSO growth. These coordinated mean-state changes collectively enhance the efficiency of the Bjerknes feedback, with the thermocline feedback (α) providing a particularly important contribution. Consequently, ENSO variability reaches its maximum amplitude near the 270° precession phase. In contrast, the opposite mean-state configuration during the 90° phase reverses these processes, resulting in reduced coupling efficiency and the weakest ENSO variability. Therefore, our study extends the classical framework of externally forced ENSO variability by identifying the specific pathway through which precession reorganizes the tropical mean state and by highlighting the important role of Indo-Pacific upper-ocean warm water structure in regulating ENSO coupling sensitivity.

A key advance of this study is the clarification of the physical pathway through which precessional forcing reorganizes tropical mean-state conditions. Previous studies have attributed the reduced ENSO activity during the Early-Middle Holocene to a suite of tropical Pacific background-state changes, including intensified Asian summer monsoon , enhanced circulation (Liu et al., 2000), an enhanced zonal Walker circulation (White et al., 2018; Dang et al., 2020), intensified stronger equatorial trade winds (Pausata et al., 2017), stronger increased eastern Pacific upwelling , a larger Pacific east–west (White et al., 2018; Lu et al., 2019), a westward-displaced ITCZ (Pontes et al., 2022), an intensified zonal SST gradient (Sadekov et al., 2013), and subduction of warm subtropical waters enhanced subtropical warm-water subduction into the equatorial thermocline . Yet, the causal links among these factors, particularly how precession-driven insolation shapes the mean state to modulate ENSO, remain unclear . We show that asymmetric heating between the Afro-Eurasian and Australian continents, driven by different combinations of perihelion and aphelion, shifts the ITCZ zonally, which service as a fundamental forcing for ENSO behaviors. This zonal displacement of the ITCZ and IPWP alters the background climate, modulating the threshold for ENSO events and ultimately affects ENSO activity. Unlike previous studies that focus on individual response(L. Chen et al., 2019; Lu et al., 2025). However, these atmospheric and oceanic mean-state variables are strongly coupled and co-vary under the influence of multiple external forcings (P. N. DiNezio et al., 2012; N. Wang et al., 2024), making it challenging to isolate the direct role of precession and determine the pathway linking orbital forcing to tropical Pacific reorganization. Based on high-resolution simulations spanning a complete precession cycle, we demonstrate that these previously identified, seemingly independent mean-state adjustments originate from a common dynamical source: precession-induced hemispheric asymmetric continental heating. This mechanism establishes a direct physical connection between orbital insolation forcing and tropical Pacific mean-state evolution, providing a unified explanation for how precession affects ENSO variability.

Furthermore, our results mechanistically link precession-driven asymmetric continental heating to the tropical Pacific mean state, which affect the threshold for ENSO development, thus regulate the demonstrate that external forcing does not regulate ENSO variability simply by shifting the mean climate state toward an El Niño-like or La Niña-like background condition (Okumura et al., 2011; P. N. DiNezio et al., 2012). Instead, ENSO variabilities. Our results indicate that we are currently experiencing a period of strong ENSO activity in the astronomical cycle. Against the anthropogenic induced increased ENSO activities , this astronomical forcing will likely suppress ENSO activity in the long-term future. Importantly, the identified mechanism—based on asymmetric continental thermal heating—offers a novel pathway for modulating ENSO variability. Under global warming, anthropogenic forcing has intensified heating over the vast Afro-Eurasian landmass. This enhanced land heating on the western side variability is primarily controlled through changes in the efficiency of ocean–atmosphere coupling within the tropical Pacific mean state. This mechanism shares fundamental similarities with ENSO responses under anthropogenic warming. Previous studies suggest that greenhouse warming may intensify ENSO variability by strengthening upper-ocean stratification (Cai et al., 2018; Tuckman & Yang, 2026), promoting an eastward expansion of the IPWP (Thirumalai et al., 2024; Molina et al., 2026), weakening the Walker circulation and equatorial trade winds (P. DiNezio et al., 2011; P. N. DiNezio et al., 2013), and modifying the structure of wind stress anomalies (Stuivenvolt-Allen et al., 2025), thereby enhancing the Bjerknes feedback and increasing the intensity and/or frequency of extreme ENSO events (P. DiNezio et al., 2010). Although precessional forcing and anthropogenic greenhouse forcing differ fundamentally in their external origins, both influence ENSO through a common dynamical pathway: reorganizing the tropical Pacific background state and modifying the efficiency of coupled ocean–atmosphere feedback (P. N. DiNezio et al., 2012; Fedorov et al., 2020; Cai et al., 2021). Under the 270° precession configuration, eastward migration of the IPWP ~~, which may contribute to a westward shift of both the ITCZ and the IPWP. Indeed, modern observations show that the Pacific mean state has shifted toward a more La Niña–like pattern in the past four decades, characterized by a westward-displaced Walker Circulation compared to the pre-Industrial period . Incorporating this~~ and Walker circulation, decreased western–central Pacific WWV, a shallower mixed layer and intensified upper-ocean stratification reduce the thermal inertia of the western Pacific warm pool. This allows modest climatic perturbations to initiate stronger Bjerknes feedback and consequently promotes heightened ENSO variability. This explains why ENSO variability reaches its maximum amplitude under the modern-like precession configuration relative to other phases within the simulated precession cycle. Therefore, our results provide a broader perspective for understanding how variations in climate mean states regulate ENSO variability across different external forcing scenarios.

In summary, this study identifies precession-driven asymmetric continental thermal forcing ~~into models of tropical climate variability may enhance the ability to predict ENSO behavior under future warming scenarios and improve climate resilience for associated extreme events~~as a fundamental driver of tropical Indo-Pacific mean-state reorganization and further demonstrates that changes in IPWP position, upper-ocean stratification, thermocline feedback, and the overall Bjerknes feedback system constitute key dynamical pathways through which ENSO variability responds to background climate changes. The proposed mechanism, linking orbital forcing to mean-state adjustment, air–sea coupling efficiency, and ENSO amplitude modulation, advances our understanding of astronomical-scale ENSO evolution and provides a physically based framework for interpreting ENSO responses under future climate change scenarios and associated changes in climate extremes.

Acknowledgments

This research was jointly supported by the construction fund of the Frontier Research Center at the Southern Marine Science and Engineering Guangdong Laboratory (Zhuhai) (No. SML2023SP204), the National Natural Science Foundation of China (42206256)~~, and Ocean Negative Carbon Emissions (ONCE)~~.

Open Research

Model output data used in this study are publicly available at the Zenodo repository (Yang, 2024). Proxy data are available from PANGAEA (https://www.pangaea.de) and the NOAA NCEI Paleoclimatology database (https://www.ncei.noaa.gov/products/paleoclimatology), with detailed dataset information provided in Supplementary Tables~~S1–S2~~ S1–S2.

Conflict of Interest

The authors declare no conflicts of interest relevant to this study.

Author Contributions

H.Y. conceived the study and conducted the AWI-ESM simulations. Y.L. performed data analyses, contributed theoretical insights, and compiled geological proxy datasets. Y.L. and H.Y. wrote the initial manuscript draft. All authors contributed to the interpretation, discussion, and revision of the paper.

References

An, S.-I., Im, S.-H., & Jun, S.-Y. (2018). Changes in ENSO activity during the last 6,000 years modulated by background climate state. *Geophysical Research Letters*, *45*(5), 2467–2475.

Barr, C., Tibby, J., Leng, M., Tyler, J., Henderson, A., Overpeck, J., ... others (2019). Holocene El Niño–Southern Oscillation variability reflected in subtropical Australian precipitation. *Scientific Reports*, *9*(1), 1627.

Bjerknes, J. (1966). A possible response of the atmospheric hadley circulation to equatorial anomalies of ocean temperature. *Tellus*, *18*(4), 820–829.

Bjerknes, J. (1969a). Atmospheric teleconnections from the equatorial Pacific. *Monthly weather review*, *97*(3), 163–172.

Bjerknes, J. (1969b). Atmospheric teleconnections from the equatorial pacific. *Monthly Weather Review*, *97*(3), 163–172. doi: 10.1175/1520-0493(1969)097⟨0163:ATFTEP⟩2.3.CO;2

Braconnot, P., Luan, Y., Brewer, S., & Zheng, W. (2012). Impact of earth's orbit and freshwater fluxes on Holocene climate mean seasonal cycle and ENSO characteristics. *Climate dynamics*, *38*, 1081–1092.

Brown, J., Collins, M., & Tudhope, A. (2006). Coupled model simulations of mid-Holocene ENSO and comparisons with coral oxygen isotope records. *Advances in Geosciences*, *6*, 29–33.

Brown, J., Collins, M., Tudhope, A. W., & Toniazzo, T. (2008). Modelling mid-Holocene tropical climate and ENSO variability: towards constraining predictions of future change with palaeo-data. *Climate Dynamics*, *30*, 19–36.

Bush, A. B. (1999). Assessing the impact of mid-Holocene insolation on the atmosphere-ocean system. *Geophysical Research Letters*, *26*(1), 99–102.

Cai, W., Santoso, A., Collins, M., Dewitte, B., Karamperidou, C., Kug, J.-S., ... others (2021). Changing El Niño–Southern Oscillation in a warming climate. *Nature Reviews Earth & Environment*, *2*(9), 628–644.

Cai, W., Santoso, A., Wang, G., Yeh, S.-W., An, S.-I., Cobb, K. M., ... others (2015). ENSO and greenhouse warming. *Nature Climate Change*, *5*(9), 849–859.

Cai, W., Wang, G., Dewitte, B., Wu, L., Santoso, A., Takahashi, K., ... McPhaden, M. J. (2018). Increased variability of eastern pacific el niño under greenhouse warming. *Nature*, *564*(7735), 201–206.

Chang, P., Wang, B., Li, T., & Ji, L. (1994). Interactions between the seasonal cycle and the Southern Oscillation-frequency entrainment and chaos in a coupled ocean-atmosphere model. *Geophysical Research Letters*, *21*(25), 2817–2820.

Chen, L., Zheng, W., & Braconnot, P. (2019). Towards understanding the suppressed ENSO activity during mid-Holocene in pmip2 and pmip3 simulations. *Climate Dynamics*, *53*, 1095–1110.

Chen, S., Hoffmann, S. S., Lund, D. C., Cobb, K. M., Emile-Geay, J., & Adkins, J. F. (2016). A high-resolution speleothem record of western equatorial Pacific rainfall: Implications for Holocene ENSO evolution. *Earth and Planetary Science Letters*, *442*, 61–71.

Chiang, J., Fang, Y., & Chang, P. (2009). Pacific climate change and ENSO activity in the mid-Holocene. *Journal of Climate*, *22*(4), 923–939.

clement, A. C., Seager, R., & Cane, M. (1999). Orbital controls on the El Nino/Southern Oscillation and the tropical climate. *Paleoceanography*, *14*(4), 441–456.

Clement, A. C., Seager, R., & Cane, M. A. (2000). El Niño during the mid-Holocene by changes in the earth's orbit. *Paleoceanography*, *15*(6), 731–737.

Conroy, J. L., Overpeck, J. T., Cole, J. E., Shanahan, T. M., & Steinitz-Kannan, M. (2008). Holocene changes in eastern tropical Pacific climate inferred from a galápagos lake sediment record. *Quaternary Science Reviews*, *27*(11-12), 1166–1180.

Conroy, J. L., Restrepo, A., Overpeck, J. T., Steinitz-Kannan, M., Cole, J. E., Bush, M. B., & Colinvaux, P. A. (2009). Unprecedented recent warming of surface temperatures in the eastern tropical Pacific ocean. *Nature geoscience*, *2*(1), 46–50.

Dang, H., Jian, Z., Wang, Y., Mohtadi, M., Rosenthal, Y., Ye, L., ... Kuhnt, W. (2020). Pacific Warm Pool subsurface heat sequestration modulated Walker Circulation and ENSO activity during the Holocene. *Science Advances*, *6*(42), eabc0402.

Denniston, R. F., Wyrwoll, K.-H., Polyak, V. J., Brown, J. R., Asmerom, Y., Wanamaker Jr, A. D., ... others (2013). A stalagmite record of holocene indonesian–australian summer monsoon variability from the australian tropics. *Quaternary Science Reviews*, *78*, 155–168.

Deppenmeier, A.-L., Haarsma, R. J., & Hazeleger, W. (2016). The bjerknes feedback in the tropical atlantic in cmip5 models. *Climate Dynamics*, *47*(7-8), 2691–2707. doi: 10.1007/s00382-016-2992-z

Di Carlo, I. A., Braconnot, P., Marti, O., & Elliot, M. (2021). *How is the increase in the variability of ENSO events over the last 6000 years linked to the mean state change of the tropical Pacific ocean?* (Tech. Rep.). Copernicus Meetings.

DiNezio, P., Clement, A., & Vecchi, G. (2010). Reconciling differing views of tropical pacific climate change. *Eos, Transactions American Geophysical Union*, *91*(16), 141–142.

DiNezio, P., Clement, A., Vecchi, G. A., Soden, B., Broccoli, A., Otto-Bliesner, B., & Braconnot, P. (2011). The response of the walker circulation to last glacial maximum forcing: Implications for detection in proxies. *Paleoceanography*, *26*(3).

DiNezio, P. N., Kirtman, B. P., Clement, A. C., Lee, S.-K., Vecchi, G. A., & Wittenberg, A. (2012). Mean climate controls on the simulated response of enso to increasing greenhouse gases. *Journal of climate*, *25*(21), 7399–7420.

DiNezio, P. N., Vecchi, G. A., & Clement, A. C. (2013). Detectability of changes in the walker circulation in response to global warming. *Journal of Climate*, *26*(12), 4038–4048.

Emile-Geay, J., Cobb, K. M., Carré, M., Braconnot, P., Leloup, J., Zhou, Y., ... others (2016). Links between tropical Pacific seasonal, interannual and orbital variability during the Holocene. *Nature Geoscience*, *9*(2), 168–173.

Fedorov, A. V., Hu, S., Wittenberg, A. T., Levine, A. F. Z., & Deser, C. (2020). Enso low-frequency modulation and mean state interactions. In M. J. McPhaden, A. Santoso, & W. Cai (Eds.), *El niño southern oscillation in a changing climate* (pp. 173–198). American Geophysical Union / Wiley. doi: 10.1002/9781119548164.ch8

Fedorov, A. V., & Philander, S. G. (2001). A stability analysis of tropical ocean–atmosphere interactions: Bridging measurements and theory for el niño. *Journal of Climate*, *14*(14), 3086–3101.

Guilyardi, E., Wittenberg, A., Fedorov, A., Collins, M., Wang, C., Capotondi, A., ... Stockdale, T. (2009). Understanding el niño in ocean–atmosphere general circulation models: Progress and challenges. *Bulletin of the American Meteorological Society*, *90*(3), 325–340.

Hewitt, C. D., & Mitchell, J. F. (1998). A fully coupled GCM simulation of the climate of the mid-Holocene. *Geophysical Research Letters*, *25*(3), 361–364.

Jian, Z., Wang, Y., Dang, H., Mohtadi, M., Rosenthal, Y., Lea, D. W., ... others (2022). Warm Pool ocean heat content regulates ocean–continent moisture transport. *Nature*, *612*(7938), 92–99.

Jin, F.-F., Kim, S. T., & Bejarano, L. (2006). A coupled-stability index for enso. *Geophysical Research Letters*, *33*(23), L23708. doi: 10.1029/2006GL027221

Jin, F.-F., Neelin, J. D., & Ghil, M. (1994). El niño on the devil's staircase: Annual subharmonic steps to chaos. *Science*, *264*(5155), 70–72.

Karamperidou, C., Di Nezio, P. N., Timmermann, A., Jin, F.-F., & Cobb, K. M. (2015). The response of ENSO flavors to mid-Holocene climate: Implications for proxy interpretation. *Paleoceanography*, *30*(5), 527–547.

Kienast, M., Kienast, S. S., Calvert, S. E., Eglinton, T. I., Mollenhauer, G., François, R., & Mix, A. C. (2006). Eastern Pacific cooling and Atlantic overturning circulation during the last deglaciation. *Nature*, *443*(7113), 846–849.

Koutavas, A., & Joanides, S. (2012). El Niño–Southern Oscillation extrema in the Holocene and Last Glacial Maximum. *Paleoceanography*, *27*(4).

Koutavas, A., Lynch-Stieglitz, J., Marchitto Jr, T. M., & Sachs, J. P. (2002). El Nino-like pattern in ice age tropical Pacific sea surface temperature. *Science*, *297*(5579), 226–230.

Lawman, A. E., Di Nezio, P. N., Partin, J. W., Dee, S. G., Thirumalai, K., & Quinn, T. M. (2022). Unraveling forced responses of extreme el niño variability over the holocene. *Science Advances*, *8*(9), eabm4313.

Leduc, G., Schneider, R., Kim, J.-H., & Lohmann, G. (2010). Holocene and Eemian sea surface temperature trends as revealed by alkenone and mg/ca paleothermometry. *Quaternary Science Reviews*, *29*(7-8), 989–1004.

Lee, S., L'Heureux, M., Wittenberg, A. T., Seager, R., O'Gorman, P. A., & Johnson, N. C. (2022). On the future zonal contrasts of equatorial Pacific climate: Perspectives from observations, simulations, and theories. *Npj Climate and Atmospheric Science*, *5*(1), 82.

Linsley, B. K., Rosenthal, Y., & Oppo, D. W. (2010). Holocene evolution of the indonesian throughflow and the western Pacific Warm Pool. *Nature Geoscience*, *3*(8), 578–583.

Liu, Z., Brady, E., & Lynch-Stieglitz, J. (2003). Global ocean response to orbital forcing in the Holocene. *Paleoceanography*, *18*(2).

Liu, Z., Kutzbach, J., & Wu, L. (2000). Modeling climate shift of El Nino variability in the Holocene. *Geophysical Research Letters*, *27*(15), 2265–2268.

Liu, Z., Lu, Z., Wen, X., Otto-Bliesner, B. L., Timmermann, A., & Cobb, K. M. (2014). Evolution and forcing mechanisms of El Niño over the past 21,000 years. *Nature*, *515*(7528), 550–553.

Loubere, P., Richaud, M., Liu, Z., & Mekik, F. (2003). Oceanic conditions in the eastern equatorial Pacific during the onset of ENSO in the Holocene. *Quaternary Research*, *60*(2), 142–148.

Lu, Z., Liu, Z., Chen, G., & Guan, J. (2019). Prominent precession band variance in ENSO intensity over the last 300,000 years. *Geophysical Research Letters*, *46*(16), 9786–9795.

Lu, Z., Liu, Z., Zhu, J., & Cobb, K. M. (2018). A review of paleo El Niño-Southern Oscillation. *Atmosphere*, *9*(4), 130.

Lu, Z., Schultze, A., Carré, M., Brierley, C. M., Hopcroft, P. O., Zhao, D., . . . others (2025). *Enhanced frequency of multi-year El Niño-Southern Oscillation across the Holocene* (Tech. Rep.). Copernicus Meetings.

Luan, Y., Braconnot, P., Yu, Y., Zheng, W., & Marti, O. (2012). Early and mid-Holocene climate in the tropical Pacific: seasonal cycle and interannual variability induced by insolation changes. *Climate of the Past*, *8*(3), 1093–1108.

Lübbecke, J. F., & McPhaden, M. J. (2013). A comparative stability analysis of atlantic and pacific niño modes. *Journal of Climate*, *26*(16), 5965–5980. doi: 10.1175/JCLI-D-12-00758.1

McGregor, H. V., & Gagan, M. K. (2004). Western Pacific coral δo18 records of anomalous Holocene variability in the El Niño–Southern Oscillation. *Geophysical Research Letters*, *31*(11).

Milankovitch, M. (1941). Canon of insolation and the iceage problem. *Koniglich Serbische Akademice Beograd Special Publication*, *132*.

Molina, B. A., DiNezio, P. N., & Deser, C. (2026). Changes in enso oscillatory dynamics associated with zonal shifts in air–sea coupling region. *Journal of Climate*, *39*(13), 3631–3652.

Moy, C. M., Seltzer, G. O., Rodbell, D. T., & Anderson, D. M. (2002). Variability of El Niño/Southern Oscillation activity at millennial timescales during the Holocene epoch. *Nature*, *420*(6912), 162–165.

Neelin, J. D., & Held, I. M. (1987). Modeling tropical convergence based on the moist static energy budget. *Monthly Weather Review*, *115*(1), 3–12.

Okumura, Y. M., Ohba, M., Deser, C., & Ueda, H. (2011). A proposed mechanism for the asymmetric duration of el niño and la niña. *Journal of climate*, *24*(15), 3822–3829.

Otto-Bliesner, B. L. (1999). El Nino/la nina and sahel precipitation during the middle Holocene. *Geophysical Research Letters*, *26*(1), 87–90.

Otto-Bliesner, B. L., Brady, E. C., Shin, S.-I., Liu, Z., & Shields, C. (2003). Modeling El Niño and its tropical teleconnections during the last glacial-interglacial cycle. *Geophysical Research Letters*, *30*(23).

Pausata, F. S., Zhang, Q., Muschitiello, F., Lu, Z., Chafik, L., Niedermeyer, E. M., ... Liu, Z. (2017). Greening of the Sahara suppressed ENSO activity during the mid-Holocene. *Nature Communications*, *8*(1), 16020.

Pontes, G. M., Taschetto, A. S., Sen Gupta, A., Santoso, A., Wainer, I., Haywood, A. M., ... others (2022). Mid-pliocene el niño/southern oscillation suppressed by pacific intertropical convergence zone shift. *Nature Geoscience*, *15*(9), 726–734.

Rackow, T., Goessling, H. F., Jung, T., Sidorenko, D., Semmler, T., Barbi, D., & Handorf, D. (2018). Towards multi-resolution global climate modeling with echam6-FESOM. part II: climate variability. *Climate Dynamics*, *50*, 2369–2394.

Roberts, W. H. G., et al. (2007). *An investigation into the causes for the reduction in the variability of the El Nino-Southern Oscillation in the Early Holocene in a global climate model* (Unpublished doctoral dissertation). University of Washington Seattle.

Rodbell, D. T., Seltzer, G. O., Anderson, D. M., Abbott, M. B., Enfield, D. B., & Newman, J. H. (1999). An˜ 15,000-year record of El Niño-driven alluviation in southwestern ecuador. *Science*, *283*(5401), 516–520.

Sadekov, A. Y., Ganeshram, R., Pichevin, L., Berdin, R., McClymont, E., Elderfield, H., & Tudhope, A. W. (2013). Palaeoclimate reconstructions reveal a strong link between El Niño-Southern Oscillation and tropical pacific mean state. *Nature communications*, *4*(1), 2692.

Salau, O., Schneider, B., Park, W., Khon, V., & Latif, M. (2012). Modeling the ENSO impact of orbitally induced mean state climate changes. *Journal of Geophysical Research: Oceans*, *117*(C5).

Sandweiss, D. H., Maasch, K. A., Burger, R. L., Richardson III, J. B., Rollins, H. B., & A. (2001). Variation in Holocene El Niño frequencies: Climate records and cultural consequences in ancient peru. *Geology*, *29*(7), 603–606.

Sandweiss, D. H., Richardson III, J. B., Reitz, E. J., Rollins, H. B., & Maasch, K. A. (1996). Geoarchaeological evidence from peru for a 5000 years BP onset of El Niño. *Science*, *273*(5281), 1531–1533.

Sha, L., Dang, H., Wang, Y., Wassenburg, J. A., Baker, J. L., Li, H., ... others (2024). Triple oxygen isotope reveals insolation-forced tropical moisture cycles. *Science Advances*, *10*(37), eadp7855.

Shulmeister, J., & Lees, B. G. (1995). Pollen evidence from tropical Australia for the onset of an ENSO-dominated climate at c. 4000 BP. *The Holocene*, *5*(1), 10–18.

Sidorenko, D., Rackow, T., Jung, T., Semmler, T., Barbi, D., Danilov, S., ... others (2015). Towards multi-resolution global climate modeling with echam6–FESOM. part i: model formulation and mean climate. *Climate Dynamics*, *44*, 757–780.

Stuivenvolt-Allen, J., Fedorov, A. V., Fu, M., & Heede, U. (2025). Widening of wind stress anomalies amplifies enso in a warming climate. *Journal of Climate*, *38*(2), 497–512.

Thirumalai, K., DiNezio, P. N., Partin, J. W., Liu, D., Costa, K., & Jacobel, A. (2024). Future increase in extreme el niño supported by past glacial changes. *Nature*, *634*(8033), 374–380.

Thompson, D. M., Conroy, J. L., Collins, A., Hlohowskyj, S. R., Overpeck, J. T., Riedinger-Whitmore, M., ... others (2017). Tropical Pacific climate variability over the last

6000 years as recorded in bainbridge crater lake, galápagos. *Paleoceanography*, *32*(8), 903–922.
Tian, Z., Li, T., Jiang, D., & Chen, L. (2017). Causes of ENSO weakening during the mid-Holocene. *Journal of Climate*, *30*(17), 7049–7070.
Timmermann, A., Lorenz, S., An, S., A., & Xie, S. (2007). The effect of orbital forcing on the mean climate and variability of the tropical Pacific. *Journal of Climate*, *20*(16), 4147–4159.
Timmermann, A., Oberhuber, J., Bacher, A., Esch, M., Latif, M., & Roeckner, E. (1999). Increased el niño frequency in a climate model forced by future greenhouse warming. *Nature*, *398*(6729), 694–697.
Trenberth, K. E., & Stepaniak, D. P. (2001). Indices of El Niño evolution. *Journal of climate*, *14*(8), 1697–1701.
Tuckman, P., & Yang, D. (2026). The rise and fall of enso in a warming world: Insights from a lag-linear model. *arXiv preprint arXiv:2603.03458*.
Tudhope, A. W., Chilcott, C. P., McCulloch, M. T., Cook, E. R., Chappell, J., Ellam, R. M., ... Shimmield, G. B. (2001). Variability in the El Niño-Southern Oscillation through a glacial-interglacial cycle. *Science*, *291*(5508), 1511–1517.
Tziperman, E., Stone, L., Cane, M. A., & Jarosh, H. (1994). El niño chaos: Overlapping of resonances between the seasonal cycle and the pacific ocean-atmosphere oscillator. *Science*, *264*(5155), 72–74.
Wang, C., Deser, C., Yu, J.-Y., DiNezio, P., & A. (2017). El Niño and Southern Oscillation (enso): a review. *Coral reefs of the eastern tropical Pacific: Persistence and loss in a dynamic environment*, 85–106.
Wang, C., & Picaut, J. (2004). Understanding ENSO physics—a review. *Earth's Climate: The Ocean–Atmosphere Interaction, Geophys. Monogr*, *147*, 21–48.
Wang, N., Dee, S., Hu, J., Steiger, N., & Thirumalai, K. (2024). Pdo and amo modulation of the enso–asian summer monsoon teleconnection during the last millennium. *Journal of Geophysical Research: Atmospheres*, *129*(1), e2023JD039638.
White, S. M., Ravelo, A. C., & Polissar, P. J. (2018). Dampened El Niño in the Early and mid-Holocene due to insolation-forced warming/deepening of the thermocline. *Geophysical Research Letters*, *45*(1), 316–326.
Yang, H. (2024). AWI-ESM precessional cycle simulation [Dataset]. Zenodo. https://doi.org/10.5281/zenodo.13681177.
Yang, H., Liu, Y., Pinho, T. M., Shi, X., Zhong, Y., Liu, Q., ... others (2025). Changing earth-sun distance drifts global circulation patterns. *Geophysical Research Letters*, *52*(4), e2024GL113066.
Yang, H., Shi, X., Wang, X., Liu, Q., Zhong, Y., Liu, X., ... others (2024). Precession driven low-latitude hydrological cycle paced by shifting perihelion. *EGUsphere*, *2024*, 1–21.
Zhang, Y., Wallace, J. M., & Battisti, D. S. (1997). ENSO-like interdecadal variability: 1900–93. *Journal of climate*, *10*(5), 1004–1020.
Zheng, W., Braconnot, P., Guilyardi, E., Merkel, U., & Yu, Y. (2008). ENSO at 6ka and 21ka from ocean–atmosphere coupled model simulations. *Climate Dynamics*, *30*, 745–762.
Zhou, P., Yan, H., Han, T., Liu, C., Yang, H., Luo, F., ... others (2022). Mid to late holocene ENSO variability reconstructed by high-resolution tridacna sr/ca records from the northern part of the South China Sea. *Palaeogeography, Palaeoclimatology, Palaeoecology*, *601*, 111117.